NANO LETTERS

2008
Vol. 8, No. 4
1081-1089

Solvent-Assisted Patterning of Polyelectrolyte Multilayers and Selective Deposition of Virus Assemblies

Pil J. Yoo,[†] Ki Tae Nam,[‡,§] Angela M. Belcher,[‡,§,||] and Paula T. Hammond*[,§,⊥]

Department of Chemical Engineering and SKKU Advanced Institute of Nanotechnology (SAINT), Sungkyunkwan University, Suwon 440-746, Republic of Korea, Department of Materials Science and Engineering, Institute for Soldier Nanotechnologies, Biological Engineering Division, Department of Chemical Engineering, Massachusetts Institute of Technology, Cambridge, Massachusetts 02139

Received November 25, 2007; Revised Manuscript Received January 30, 2008

ABSTRACT

We introduce a simple method to pattern electrostatic assemblies of viruses onto a polyelectrolyte multilayer. The increased mobility of weak polycation chains in the multilayer above a given thickness ensures the surface mobility of viruses required for spontaneous ordering of densely packed viruses atop polymeric patterns. To pattern the polyelectrolyte multilayer film, we employ a nonconventional patterning method known as solvent-assisted capillary molding for the first time on multilayer films, and demonstrate micrometer-scaled dense patterns of viruses, where the accessible feature size can be correlated by the length scale of virus and swelling property of underlying patterned polyelectrolyte multilayer. We further examine the ability to modify the top surfaces of these assemblies with biological ligands, which extends the applicability of patterned viruses to biological detection purposes. We expect that the present method described here can be generally applied to the patterning of other polyelectrolyte multilayers and combined with the ordered assembly of anisotropic nanomaterials such as polymeric nanotubes or inorganic nanowires for a broad range of applications.

The spatial control and arrangement of anisotropic nanomaterials has received much attention due to its great technological and scientific significance, resulting in various applications ranging from molecular nanoelectronics to biological sensing devices.[1–3] The patterning of nanomaterials has also provided a fundamental strategy in designing building blocks that facilitate hierarchical supramolecular self-assembly.[4,5] This versatility arises from the ability to achieve high degrees of geometrical anisotropy (aspect ratios of 10−100) along with unique material properties. Among the several patterning techniques that have been proposed, methods that combine patterned chemical templates with physical interactions have enabled substantial success in positioning a targeted single nanowire or collectively functionalized nanowires or nanotubes onto desired locations.[6–11] However, obtaining control over patterned anisotropic nanomaterials to generate dense and ordered structures has been challenged by some inherent drawbacks, such as strong nonspecific interactions and increased steric effects.

The genetically engineered M13 virus is a new class of anisotropic biomaterial that can bridge the flexibility, precision, and chemical diversity of biomolecules with the practical applicability of inorganic nanowires. The M13 bacteriophage is a virus that only infects bacteria and is composed of ∼2700 major coat proteins helically stacked around its single-stranded DNA, yielding a monodisperse and semiflexible filamentous structure.[12] Through modification of the M13 genome, coat proteins at varying regions of the virus can be engineered to have heterofunctionality with specific binding to inorganic nanomaterials. Moreover, the monodispersity and anisotropy of the M13 virus allows the construction of highly dense and ordered nanostructures.[13,14] To pattern M13 viruses onto specific locations, utilization of covalent or biological binding with a chemically patterned template has been employed.[15] Patterning other viruses via coordination chemistry has also been studied, mostly combined with the dip-pen nanolithographic technique, and successful progress was demonstrated in realizing viral

* Corresponding author: hammond@mit.edu
[†] Department of Chemical Engineering and SKKU Advanced Institute of Nanotechnology (SAINT), Sungkyunkwan University.
[‡] Department of Materials Science and Engineering, Massachusetts Institute of Technology.
[§] Institute for Soldier Nanotechnologies, Massachusetts Institute of Technology.
[||] Biological Engineering Division, Massachusetts Institute of Technology.
[⊥] Department of Chemical Engineering, Massachusetts Institute of Technology.

10.1021/nl073079f CCC: $40.75
Published on Web 03/21/2008

nanoarray patterns.[16–20] Despite the advantage of precise patterning down to the nanometer scale, probe-based serial processing is relatively slow, discouraging the use of large substrates and areas. Furthermore, such lithographic approaches require advanced equipment and capabilities and do not enable the direct patterning of relatively complex composite structures such as multilayer thin films with desired functionality.

The electrostatic layer-by-layer assembly technique is an alternating deposition method between complementary charged species, which allows the creation of functional thin films and highly tunable surfaces through the control of electrostatic interactions.[21,22] Recently, we developed a novel method for the self-assembly of M13 viruses by employing the unique phenomenon of polymeric interduffusion, which is observed in some layer-by-layer (LbL) assembled polyelectrolyte multilayers (PEMs). In this approach, the competitive electrostatic binding between oppositely charged polyelectrolytes resulted in the segregation of virus molecules from the bulk of a multilayer film to the multilayer surface, yielding a two-dimensional ordered monolayer assembly of M13 viruses.[23] Further biotemplating of the engineered M13 virus can convert an M13 virus monolayer into an assembly of cobalt oxide nanowires, which can be utilized for a virus-based electrode for lithium-ion batteries.[24] The combination of electrostatic multilayer assembly and the virus monolayer provides a platform for the systematic integration of polymeric, biological, and inorganic materials. In an effort to advance this technology, we have investigated means of patterning LbL/ordered virus component thin films to enable additional control over the assembled structures for applications ranging from microsensing elements to microelectrodes or power microelements such as supercapacitors or batteries.

Herein, we develop a facile means of direct assembly of M13 viruses on mobility-enhanced polyelectrolyte multilayers and achieve patterned LbL/virus assemblies on surfaces using a solvent-assisted capillary molding process. Viruses are directly captured from solution onto the charged surface of a patterned polymeric template via electrostatic attraction and then ordered into closely packed monolayer structures spontaneously via the enhanced surface mobility provided from the underlying PEM patterns. By careful selection of the polyelectrolyte multilayer system such that a mobile cationic moiety of polyelectrolyte is present at the top surface, we can engage the direct ordering of negatively charged M13 viruses that present carboxylic acid groups on their protein coats atop the patterned polyelectrolyte multilayers. This approach offers excellent advantages in that target surface molecules or ligands on the virus body can be readily concentrated into highly ordered and densely packed structures without any external physical forces or additional chemical functionality. The straightforward procedure of solvent-assisted capillary molding can also be potentially utilized as an alternative and more general tool for patterning LbL assembled polymeric films over large areas without the utilization of chemically prepatterned surface chemistry[25,26] or transfer stamping methods.[27–30] Other means of generating patterns of polyelectrolyte multilayers include inkjet printing,[31] microfluidics,[32] reactive multilayers such as diazoresins for photolithography,[33] and lift-off methods.[34,35] In some of these approaches, the resolution is relatively limited due to the means of applying the pattern or the limitations of reaction-diffusion in multilayer thin films. In other cases, one must utilize repetitive steps in fluidic devices or more conventional photolithographic steps that are more expensive and less versatile. Capillary force lithography (CFL) and related approaches are soft lithographic methods that can be applied to a very broad range of flexible or rigid substrates, and two-dimensional and three-dimensional surfaces.[36] Moreover, this method enables the patterning of multilayers directly on the substrate irrespective of the thickness of the PEM film, which should prove highly beneficial for the patterning of multicomponents stacked or hybridized LbL systems. Here we investigate a subtractive means of patterning multilayers that is relatively independent of underlying surface or substrate interactions and allows the use of multilayer films in their original polyion stack ordering, which can be key in situations in which the nature and composition of the top multilayer surface is critical to the material's end use or further microfabrication steps.

Figure 1 shows a schematic illustration and representative result of direct virus assembly on a multilayer surface assembled from the alternation of linear polyethylenimine (LPEI) and poly(acrylic acid) (PAA), inspired from the previously reported methods of interdiffusion-induced virus ordering.[23,24] LPEI is a weakly charged polyelectrolyte with a relatively hydrophilic backbone that can enable interdiffusion and ordering mobility, as confirmed by superlinear growth in film thickness during LbL deposition.[37–39] When charged viruses are adsorbed onto a thin multilayer film (usually less than 10 nm, 2.5 or 3.5 bilayers of LPEI/PAA) with LPEI as the positively charged top surface as shown in Figure 1A, they are electrostatically bound but kinetically frozen on the surface due to the lack of surface mobility of the viruses on the relatively compact first few bilayers of the multilayer thin film. The mobility in the initial, thinner layers is typical of a multilayer with relatively two-dimensional well-spread polyelectrolyte chain conformations that would be fairly constrained at the top surface; there is also the possibility of a substrate effect on the top polycation layer from the negatively charged nonconformable solid silicon oxide surface underlying the multilayer film when it is very thin. In our previous studies, we found that additional LPEI/PAA multilayers can be directly adsorbed onto the virus/multilayer stack to induce the polymeric interdiffusion of LPEI and exchange between the virus and PAA in the *z*-direction, simultaneously providing the mobility needed for the viruses to achieve an ordered, highly packed arrangement on the top surface. Alternatively, upon adsorbing viruses to a much thicker PEM (usually thicker than 100 nm, more than 10.5 bilayers of LPEI/PAA) as depicted in Figure 1C, the increased surface mobility of the underlying polycation layer enables the spontaneous ordering of viruses immediately upon adsorption to the top surface (Figure 1D). For the first several layers of deposition, LPEI/PAA multilayers grow

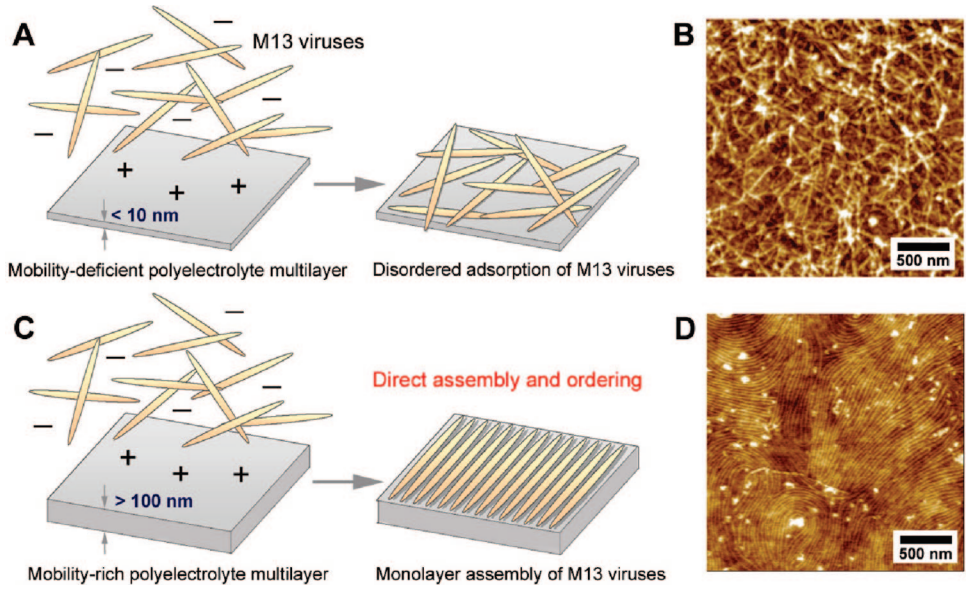

Figure 1. Comparison between low-mobility and high-mobility surfaces of polyelectrolyte multilayer for virus adsorption and ordering. (A) Scheme for random virus adsorption on very thin and mobility-deficient PEM surface. (B) Height-mode atomic force microscopic (AFM) image for A (scan size = 3 × 3 μm^2, *Z*-range = 20 nm). Viruses are adsorbed on $(LPEI/PAA\ 5.0/5.0)_{3.5}$ of 8 nm thickness. (C) Scheme for directly ordered viral assembly on relatively thick and mobility-rich PEM surface. (D) Height-mode AFM image for C (scan size = 3 × 3 μm^2, *Z*-range = 5 nm). Viruses are adsorbed on $(LPEI/PAA\ 5.0/5.0)_{10.5}$ of 130 nm thickness.

exponentially, with much thinner layers in the first few bilayer cycles and increasingly thicker layers of both PAA and LPEI with each subsequent layer. This phenomenon is due to the fact that these multilayers undergo interdiffusion of polyelectrolytes during the assembly process, as described in detail by other researchers as well as our own group in separate papers.[37–39] The thinner films formed initially consist of much more confined polyelectrolyte layers that present a thinner "monolayer" of LPEI on the top surface. As the number of bilayers increases, the top LPEI layer becomes increasingly thicker, with less interpenetration with the underlying polyion layer and greater mobility of the film at the top surface. The major difference between this method as compared to the previous one,[23] is that the variation in the thickness of the free diffusing species (LPEI) on the surface can lead to a dramatic change in the lateral mobility of the polyelectrolyte, which is manifest in the spontaneous ordering and assembly behavior of viruses at the top surface.

The relative mobility of LPEI under the conditions of adsorption is important, as this kind of ordering is not observed with strong polyelectrolyte pairs or with more basic polycations such as poly(allylamine hydrochloride), which contains primary amines with a higher pK_a.[40] The lower degree of ionization, as well as the relatively hydrophilic polymer backbone of LPEI, may enable a greater amount of surface mobility when it is adsorbed as the top layer in thicker multilayer films.

The result of the direct assembly is a densely packed monolayer structure of viruses as shown in Figure 1D. Surface-adsorbed viruses are mobilized on the polyelectrolyte multilayer and spontaneously rearrange to an ordered monolayer structure aided by their inherent liquid-crystalline tendency to close-body pack. After the surface charge becomes overcompensated on the surface, further deposition of virus molecules is prevented due to charge repulsion, which enables quantitative control over assembly density depending on the surface charge density of the virus. As compared to the previously reported method based on in situ interdiffusion,[23] where virus adsorption and polyelectrolyte deposition were achieved concurrently, the added advantage of this direct virus adsorption assembly approach is that it allows independent manipulation of LbL deposition and virus incorporation and ordering. By utilizing prepatterned multilayers to generate a template for selective charge binding, it is possible to accomplish the construction of patterned virus assemblies in a reliable fashion.

Polymeric molding processes are an efficient way of generating physically patterned polymeric structures. Among several approaches, capillary force lithography is a candidate that utilizes the fluidic mobility of polymers at high temperature conditions (above the T_g of the polymer) to induce molding. When the sample is heated above the T_g, the subsequently generated capillary rise of polymer within the channel patterns of a PDMS mold or stamp acts as a driving force to mold and pattern the polymeric film.[36,41,42] Using thermal mobility, however, is not applicable to most LbL assembled film systems because in the dry state the ionic complexes might be considered networks based on multivalent ionic cross-links that impede flow and, furthermore, the heating of polyacid/polyamine multilayers to high temperatures usually brings about thermal cross-linking between cationic and anionic species.[43,44] To overcome this challenge, instead of utilizing thermally induced mobility, we turned to another means of achieving polymeric mobility via softening of the multilayer film with suitable solvents. Such

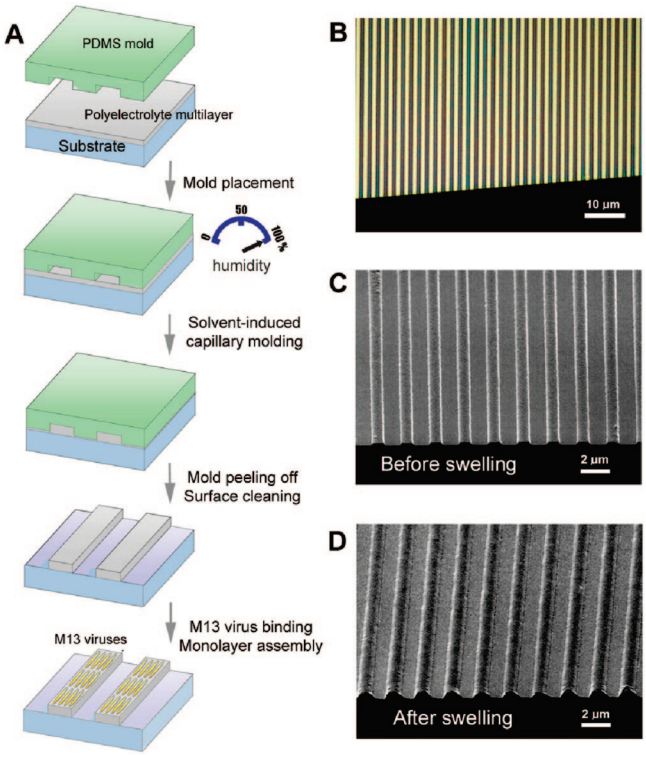

Figure 2. Solvent-assisted capillary molding technique. (A) Schematic illustration of the experimental procedure. M13 viruses are selectively bound and ordered on the patterned surface of a polyelectrolyte multilayer. (B) Optical micrograph for 1 μm line-and-space patterned LPEI/PAA multilayer from solvent-assisted capillary molding. Viruses are not assembled in this step. (C) SEM image of pattern in B. Tilted observation shows well-defined and highly anisotropic pattern edges. (D) SEM image of a pattern after a treatment of water immersion. Cross-sectional image reveals that patterns are deformed and rounded to have isotropic and droplet-like shapes.

methods have not yet been reported for the patterning of polyelectrolyte multilayers.[45,46]

A schematic procedure for solvent-assisted capillary molding is shown in Figure 2A. First, a PEM of LPEI and PAA was deposited by conventional LbL assembly process on a targeted substrate. To induce capillarity, samples were placed in a closed container at a mildly elevated temperature (normally at 80 °C) with a water reservoir, from which the water was evaporated to achieve saturated vapor pressure. The polyelectrolyte multilayer film became swollen due to moisture uptake (34% of volume expansion was observed under 100% relative humidity condition at 80 °C). The water acts as a plasticizer and enables the multilayer to soften at elevated temperature; furthermore, it is possible under such conditions to encourage re-formation of ionic bonds as the polymer film is compressed during the molding process. A patterned poly(dimethylsiloxane) (PDMS) stamp was then conformally applied atop the PEM film with a pressure of a few bars, which ensured conformal contact with the stamp and accelerated the rate of capillary rise within the mold, thus reducing processing time (from at least 1 day to less than several hours).[42] Capillarity took place with the PDMS mold channel patterns via the flow of polymer to fill the void space of the PDMS pattern, ultimately leading to the generation of negatively replicated structures of the polymer on the surface (Figure 2B). Careful control of the initial film thickness of the PEM to account for the surface-to-volume ratio of the PDMS mold pattern could ideally lead to the formation of a completely filled mold without leaving any residual polymer in the interstitial regions between the molded features. In this case, however, a hydrophilic charged substrate was commonly used to promote the stable film deposition of polyelectrolytes; thus, a very thin residual layer (less than a few nanometers) of polyelectrolyte is retained due to strong interfacial interactions with the substrate, which consequently hinders the complete dewetting of the PEM film from the substrate.[47,48] Therefore, the conventional method of plasma cleaning was slightly employed for 30 s to eliminate this thin residual layer, exposing the original substrate underneath. (See details in Experimental Section.) This plasma treatment is kept brief to ensure that the top surface of PEM patterns retains an excess amount of positively charged LPEI, which enables further binding and assembly of M13 viruses atop the surface of LPEI. Finally, negatively charged M13 viruses were applied and selectively bound on the patterned template of the PEM, completing the process for the patterned LbL virus monolayer assembly.

The structures described above were imaged at each step using scanning electron microscopy (SEM). As seen from Figure 2C, the polymeric pattern obtained immediately after the mold removal shows well-defined structures distributed uniformly over an area of several square centimeters. When the patterned polyelectrolyte multilayers are eventually exposed to an aqueous environment a second time to adsorb viruses from solution, the physically patterned PEM structures undergo a swelling deformation in water. To determine the influence of swelling, the pattern in Figure 2C was immersed in water for an hour and checked with SEM. As shown in Figure 2D, the original anisotropically edged patterns were deformed to isotropically rounded shapes clearly seen from the cross-sectional image, which is characteristic of fluidic behavior of polymers in the swollen phase. In the course of swelling and subsequent deformation, there is also some lateral diffusion of the polyelectrolyte film to the adjacent void areas of the substrate between patterned lines due to favorable wetting; therefore, it is expected that the minimum feature size of patterned structures fabricated by this method can encounter a limitation down to a certain geometrical value. For densely patterned line-and-space (one-to-one ratio) structures, we identified that pattern selectivity can be stably maintained down to approximately 700 nm line widths under swollen conditions.

Prior to virus assembly on the top surface, we investigated the feasibility and the kinetics of solvent-assisted capillary molding as a function of the processing temperature and feature size of patterns. As mentioned, the water vapor treatment of the polyelectrolyte multilayer film provides a plasticization effect which leads to a decrease in the glass transition temperature (T_g), thereby lowering the viscosity of the polymer. The plasticization effect can be inferred from the following approximate relationship for T_g between

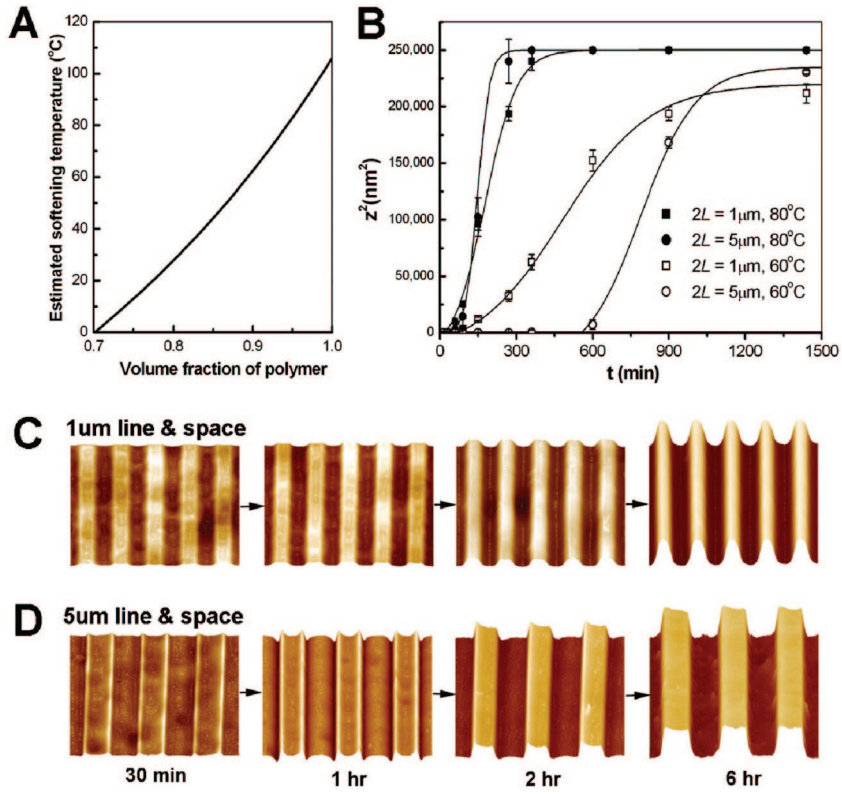

Figure 3. Correlation of solvent-assisted capillary molding with the pattern geometry and processing humidity. (A) Rough estimation of the effect of vapor addition on the glass transition temperature of the PEM film. Glass transition represents an upper bound for the multilayer film by presuming the film exhibits the glass transition of PAA and is plasticized by water. (B) Effect of pattern geometry and processing humidity on the rate of capillary rise. The initial film thickness of the PEM film is 470 nm and the cavity height of the channel patterns in the PDMS mold is 500 nm. (C, D) Experimental observations of the stepwise progress of solvent-assisted capillary molding for two different types of patterns (1 μm line-and-space for C and 5 μm line-and-space for D). Images are three-dimensional AFM images of 10 μm $\times$ 10 μm scan for C and 30 μm $\times$ 30 μm for D.

polymer and its good solvent:[49]

$$T_g \approx \frac{T_{g,p}}{1 + (X-1)(1-\Phi_p)} \quad (1)$$

where

$$X \approx T_{g,p}/T_{g,s}$$

Here, $T_{g,p}$ and $T_{g,s}$ are the glass transition temperature of the pure polymer and the solvent, respectively. Φ_p denotes the volume fraction of the polymer. It can be fairly difficult to determine the T_g of multilayer films using traditional thermal methods; attempts to find values for these systems using DSC or DMA were inconclusive. LPEI homopolymer is a highly crystalline solid, and although its amorphous regions are expected to exhibit a fairly low glass transition temperature, it is not straightforward to estimate the glass transition of the dry LPEI/PAA film, which might be considered to be a polyionic complex homogeneous blend. Rather, to get a general sense of the limiting softening temperature of the LPEI/PAA LbL films, we will use the upper bound on the glass transition temperature for this LbL matrix, which is the highest T_g of the two polyelectrolyte components, PAA. To estimate the softening temperature of LPEI/PAA complexes by the uptake of moisture, therefore, we simply used a value of $T_{g,p} = 379$ K (106 °C), which is the value for PAA homopolymer[48] and the $T_{g,s}$ of 165 K for water.[50] Figure 3A shows a predicted upper bound for the "softening temperature" with increasing water fraction, based on the above three equations. A significant lowering in this maximum softening temperature is seen to result from the uptake of water vapor solvent. For example, the LPEI/PAA multilayered film is observed to be swollen up to 34% in volume ($\Phi_p = 0.75$) under a condition of 100% relative humidity at 80 °C (0.47 atm of vapor pressure), which can yield an estimated softening temperature of 13 °C from Figure 3A. In general these rough calculations do not take into account the blend composition of LPEI with PAA or the unique nature of hydrogen bonding in plasticization of the LPEI/PAA blend with water; however, the calculations do give a more general sense of the potential impact of plasticization on this process. We can expect that this decrease in softening temperature makes the polymer more fluidic, thus enabling capillary molding into the microchannels of PDMS mold to be feasible.

We also correlated the kinetics of solvent-assisted capillary molding as a function of pattern geometry and processing humidity. For uniform flow into a channel from a film of polymer, which corresponds to the capillary system, the Poiseuille flow can be used to explain the capillary rise of the fluid, which yields[42]

$$\frac{dz}{dt} = \frac{\Delta P}{3\eta z(1/L^2 + 2/h^2)} \quad (2)$$

where z is the height of fluid rise in the channel in time, t, and ΔP is the pressure drop. L is the half-channel width, h is the time-dependent film thickness, and η is the viscosity of the fluid. Assuming the channel is open-ended (the mold is highly vapor permeable) and the film thickness is sufficiently large, eq 2 can be reduced to

$$z = \left(\frac{2L\gamma \cos\theta}{3\eta} t\right)^{1/2} \quad (3)$$

where γ is the surface tension of the polymer and θ is the equilibrium contact angle at the three-contact line. Plotting z^2 versus t, therefore, can provide a relationship between the channel filling rate and the pattern geometry (L) and processing humidity (η). As shown in Figure 3B, however, the slope dz^2/dt is not constant. Instead, the data show a tendency toward sigmoidal saturation. This saturation is attributed to two possible reasons that are typical characteristics of capillary molding: (1) initial slower or retarded capillary rise as compared to the steady-state rise, which comes from the principle that the meniscus formation of a fluid is a prerequisite for the capillary rise; (2) final slower saturation of the channel filling rate due to restrictions of the end-capped channel geometry in actual experiments. For a viscous fluidic system, it usually takes some time to form the meniscus, as shown in comparative examples in parts C and D of Figure 3. When the width of patterned channel is relatively large ($2L = 5$ μm for Figure 3D), it accordingly needs a larger meniscus to initiate a capillary rise, for which relatively longer times are required. Once the meniscus forms, however, the rate of capillary rise is much faster than that in the narrower channels, which can be clearly verified from Figure 3B.

Viscosity also strongly affects the rate of capillary rise. Because the viscosity of the polymer is directly correlated to the glass transition temperature as mentioned above, we varied the temperature while maintaining a 100% relative humidity condition. Two different temperature conditions were used, 60 and 80 °C, which correspond to 0.20 and 0.47 atm of saturated vapor pressure at 100% relative humidity, respectively. As expected, the plasticization effect is much weaker at 60 °C due to the lower amount of moisture uptake in the PEM film, which yields a slower capillary rise and a longer retardation time for the initial meniscus formation as shown in Figure 3B.

Detailed observations by atomic force microscopy (AFM) of the virus assembled PEM pattern show that viruses are uniformly ordered into monolayer structures as shown in Figure 4. We demonstrated two types of representative patterns (line in Figure 4A and dot in Figure 4B), which are potentially useful for the construction of interconnected or arrayed high-density structures in electronic and biological applications. Due to swelling in the virus solution during the virus assembly process, as discussed earlier, the PEM patterns have rounded curvature, leading to the formation of cylindrical line patterns and checkerboard-like rounded dot patterns (Figure 4, panels A and B). Interestingly, the shape of each individual dot is a volcano-like droplet instead of an ideally rounded hemispherical one. This shape might be attributed to the relatively high surface-to-volume ratio

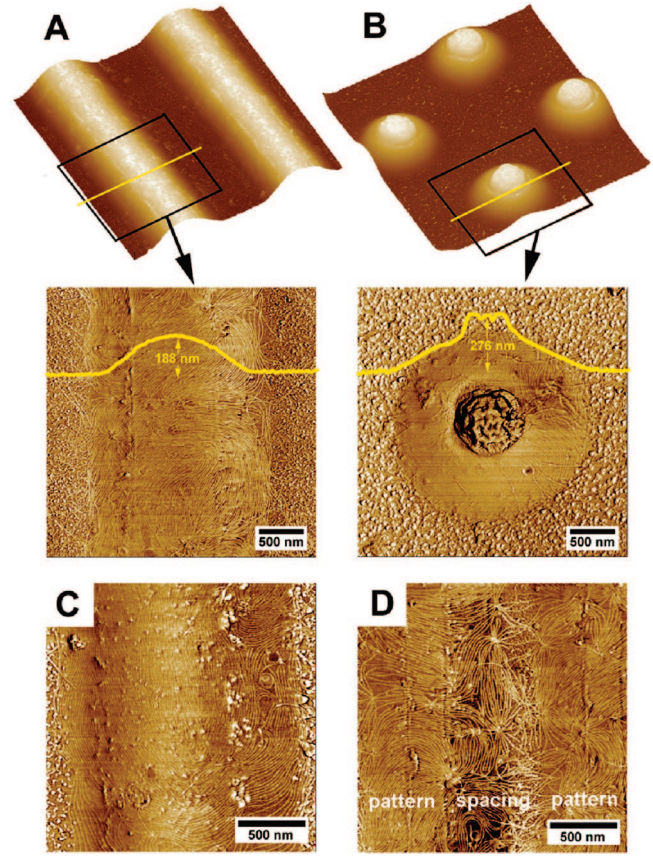

Figure 4. AFM images of patterned assembly of viruses on mobility-enhanced polyelectrolyte multilayer template. (A, B) Assembled viruses on 1.5 μm line-and-space patterns (A) and 1.5 μm spaced dot array (B). Three-dimensional AFM image (top, scan size = 6 × 6 μm^2, Z-range = 300 nm) and magnified phase-mode AFM image (bottom, scan size = 3 × 3 μm^2, Z-range = 30°) are presented and insets of yellow lines indicate the cross-sectional contour of each pattern. (C) Phase-mode AFM image of highly aligned viruses on 1.5 μm line-and-space patterns (scan size = 2 × 2 μm^2, Z-range = 40°). (D) Phase-mode AFM image of randomly ordered viruses on 1.0 μm spaced line patterns (scan size = 2 × 2 μm^2, Z-range = 40°).

of the dot pattern in the original PDMS mold, which results in swelling-induced (or drying-induced) stresses and consequent surface wrinkles at the center of the pattern.[51] Phase mode AFM images in panels A and B of Figure 4 reveal that the virus molecules are selectively adsorbed on the patterned PEM surface with a well-ordered monolayer structure. There are some small amounts of nonspecifically bound globular particles observed outside the desired patterns which could be due to the protein debris which might be generated during the virus preparation procedure. During the amplification of M13 viruses using *E. coli* bacteria, a small portion of major coat proteins of M13 viruses can fail to assemble properly, resulting in a coexistence of spherical protein particles with M13 viruses.

Closer observation of the images shows minimal nonspecific adsorption of viruses on the silicon substrate between patterns. To address this issue of nonspecific binding, we examined virus binding on a bare, plasma-cleaned silicon substrate and confirmed that there was little noticeable binding of viruses with a diluted virus solution with a

concentration ranging from 10^9 to 10^{10} molecules/mL. Moreover, the repulsive electrostatic interactions between the negatively charged M13 viruses and the plasma-treated substrate helped viruses keep from binding to the surface. More importantly, it is notable that the surface density of the viral monolayer of 30−50 viruses/μm^2 is considerably higher than the volumetric density of the virus solution of 1−10 viruses/μm^3 (10^9−10^{10} viruses/mL), which proves the advantage of this method toward an efficient integration of target molecules. The concentration of the virus solution is another important factor in determining the characteristics of ordered assembly of viruses on the surface. When the solution is too concentrated (thicker than 10^{12} molecules/mL), the amount of initial adsorption of virus is too excessive to induce the surface reordering of viruses through polymeric surface mobility from the underlying LPEI, leading to a disordered and randomly adsorbed phase of viruses. When the solution is too dilute (thinner than 10^8 molecules/mL), on the other hand, the surface assembly of viruses is entirely governed by the migration of viruses onto the surface from the solution, not by the surface mobility of underlying polymer. Such a condition yields a phase of adsorbed viruses that lacks in order as well as in assembly density.

One interesting observation is that the viruses align considerably along the edges of the pattern for both geometries (Figure 4A−C). For a parallel line pattern, viruses are moderately ordered along the axial pattern direction. For a checkerboard-like dot pattern, similarly, viruses are well ordered, with bending to conform to the curvature of dot pattern. In particular, as shown in Figure 4C, viruses appear to be ordered in a smectic liquid crystalline phase constrained by boundary-driven ordering. The highly ordered assembly of the viruses, however, can be eliminated when the pattern size is similar or less than the length scale of virus. As seen from Figure 4D (1 μm line pattern with 1 μm spacing), viruses of 1 μm in length are more randomly adsorbed on the surface. This random arrangement, as well as nonspecific adsorption on the spaces, is attributed to the fact that the initial adsorption of single viruses from the solution to the patterned polymeric surface must take place so as to allow virus contact with multiple lines and spaces in the polymeric patterns simultaneously because the length of virus is comparable to the width of the pattern spacing. Therefore, in this experiment, the minimum feature size of the virus-assembled pattern is limited to a slightly larger value than the length scale of the virus itself (around 1.5 μm line-and-spacing). With either a wider spacing or shorter length biomolecules, it is anticipated that submicrometer scaled patterning and assembly can readily be obtained while retaining close-packed order.

To test the potential of viral assembled patterns as platforms for biological sensors or analytical tools, we attached biotin to the main body of the M13 virus molecule. Biotin is a well-accepted small ligand that binds strongly to streptavidin. To attach the biotin to the M13 virus body, biotin conjugated anti-fd bacteriophage was applied, which specifically bind to major coat proteins of the M13 virus. Then, a dilute solution of Alexa Fluor conjugated streptavidin

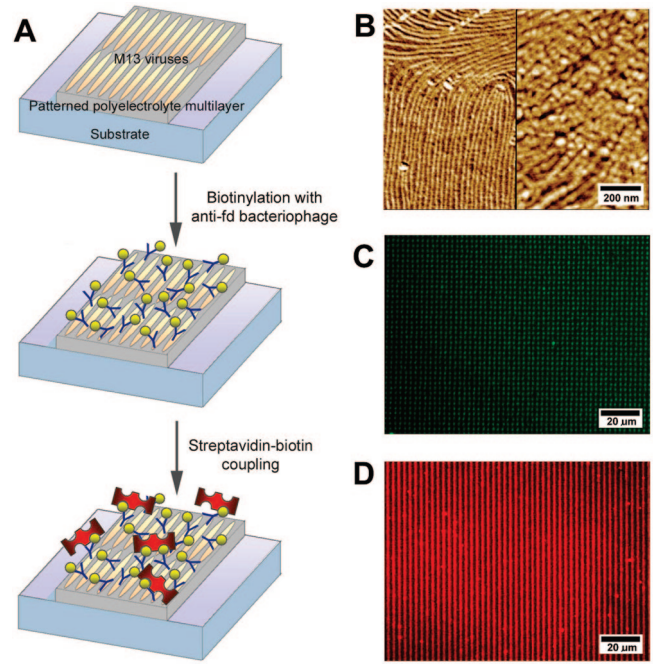

Figure 5. Demonstration of protein detection with patterned virus assembly. (A) Schematic illustration of the experimental procedure. (B) Phase mode AFM images for "before biotinylation" (left) and "after biotinylation" (right). Scan size is 600 nm × 1 μm and *Z*-range is 40°. (C) Green fluorescent image of Alexa Fluor 430 streptavidin bound viral dot array. (D) Red fluorescent image of Alexa Fluor 546 streptavidin bound viral line patterns.

(1 μg/mL) was applied onto the biotinylated pattern for less than 5 min, followed by an intensive washing in nonfluorescent medium to remove an excess or nonspecific binding. Overall procedure is schematically illustrated in Figure 5A. The successful binding of biotin onto virus coat proteins can be observed with high-resolution AFM, as shown in Figure 5B, where a closely packed structure of viruses (left) was functionalized to have biotin groups (right). Fluorescence microscopy (Figure 5C,D) reveals that streptavidin molecules are specifically bound on the patterns of biotin/virus/PEM layer. Sharp contrast in the fluorescence signal between the pattern and background surfaces proves that the streptavidin molecules were successfully recognized and captured selectively within the patterned domains. It is anticipated that further genetic engineering of viruses to express a specific peptide that can recognize the target biomolecule, combined with a reporter molecule within the multilayer or on the virus surface, can broaden the potential applications of this technique in biosensing areas.

In summary, we have presented a simple yet robust technique of direct virus assembly on a mobility-enhanced polyelectrolyte multilayer template. To pattern the polyelectrolyte multilayer film, the nonconventional patterning method of solvent-assisted capillary molding was employed for the first time with electrostatic multilayer assemblies, leading to the successful direct assembly of viruses onto the pattern. We also demonstrated the potential applicability of the technique as an analytical tool for biological recognition through appropriate manipulation of protein functionality on the virus surface. There are a number of advantages

associated with this technique for patterning other types of aniotropic nanomaterials. For example, the ability to achieve ordering of a charged nano-object atop an oppositely charged multilayer tuned to achieve high levels of surface mobility might be translated to the ordering of other charged nanoscale objects. The close-packed ordering of the viruses can take place on the surface without any additional aids such as externally applied fields or confined regions of chemical functionality. Further implementation of these systems with additional physicochemical properties can lead to the implementation of multifunctionality to the pattern or the construction of hierarchical structure. The use of environmentally friendly principles in patterning the polyelectrolyte multilayer and binding the target molecules can also provide the additional benefits of green processing and extensive versatility in substrate choice.

Experimental Section. Layer-by-Layer Deposition of Polyelectrolyte Multilayers. LPEI (25000 M_w, Polysciences) and PAA (90000 M_w, 25% aqueous solution, Polysciences) were used as-received and prepared as 35 and 20 mM solutions in deionized water, respectively, based on the repeat-unit molecular weight. The pH of both solutions was adjusted to 5.0 carefully with diluted solutions of hydrochloride and sodium hydroxide. Cleaned silicon or glass substrates were first plasma-treated to prepare an initial negatively charged surface. Polyelectrolyte multilayers were prepared using a HMS programmable slide stainer (Zeiss) with a deposition condition of 15 min adsorption of polyelectrolyte and followed by three sequential washing steps in the bath of deionized water. The nomenclature (LPEI/PAA $m/n)_X$ is used to denote a multilayer film of X layer pairs of LPEI and PAA deposited at pH m and n, respectively. When X includes 0.5, LPEI is the final adsorbed layer and thus the outermost surface of the multilayer. For the deposition of a very thin film of LPEI/PAA (less than 10 nm), 2.5 or 3.5 bilayers of LPEI/PAA, (LPEI/PAA 5.0/5.0)$_{2.5-3.5}$, were prepared. On the other hand, for a relatively thick layer of film (usually thicker than 100 nm), more than 10.5 bilayers of LPEI/PAA, (LPEI/PAA 5.0/5.0)$_{10.5\text{ or more}}$, were deposited.

Solvent-Assisted Capillary Molding. PDMS molds were fabricated by thermally casting prepolymer (Sygard 184, Dow Corning) onto the complementary relief structures of a silicon master prepared by photolithography. To thermally cure the PDMS molds, a 1:10 ratio of curing agent and the PDMS prepolymer were mixed and incubated at 70 °C for 3 h. Cured PDMS molds were then peeled from the master and cut into desired sizes. Generally, cured PDMS does not significantly take up water (less than 1 wt % of maximum water uptake), ergo it is useful for a water-based solvent-assisted capillary molding method. For solvent-assisted capillary molding, prepared samples of the LPEI/PAA film were placed in a mildly heated humid chamber (normally at 80 °C, 100% relative humidity) for 0.5 h to soften the film prior to contact with PDMS mold. Then the PDMS mold was placed onto a water vapor exposed polymeric film with a slight pressure of a few bar to promote the capillary molding. After 3−4 h, the PDMS mold was detached from the sample surface and the replicated patterns of the polyelectrolyte multilayer remained on the surface. To remove the very thin residual layers of polymer from the mold contact regions, the patterned surface was treated with 30 s of plasma cleaning (PDC-001, 18 W, Harrick Plasma), during which an air plasma was irradiated onto the sample with an etching rate of about 30 nm/min. Interstitial regions were observed with AFM, and the measured surface roughness was compared with that of a bare silicon wafer in order to verify the clean removal of residual layers.

Patterned Assembly of M13 Viruses. Wild-type M13 viruses were dispersed in water to give a dilute concentration of 10^9-10^{10} molecules/mL, and the solution pH was adjusted to 5, which is identical to the deposition pH of LPEI and PAA. Under this condition, the M13 virus can be moderately charged with negative charges (degree of ionization ~60%)[23] and can be adsorbed and ordered onto the positively charged LPEI surface. In order to induce the patterned assembly of M13 viruses on the PEM, the virus solution was drop-dispensed on prepared patterns of polymer for 20−60 min at ambient temperature. Notably, no buffer was used for the preparation of the virus solution to prevent affecting the underlying PEM patterns, which are susceptible to reorganization or dissociation in a strong ionic environment. Similarly, very careful pH adjustment of the virus solution was performed, and as a result, the total concentration of added salts from highly diluted HCl and NaOH was maintained at less than 1 mM. The resulting virus assembled pattern was rinsed with deionized water intensively to remove any excess virus and dried by blowing in nitrogen flow.

Binding of Biotin on Patterned Viruses and Subsequent Streptavidin Coupling. To attach biotin groups on assembled M13 viruses, biotin conjugated anti-fd bacteriophage (Sigma), which was developed in rabbits using repeated injections of fd bacteriophage (or M13 bacteriophage) as the immunogen, was diluted to 3−5 μg/mL in water and applied onto the patterned virus surface for 5 min, followed by 1 min of washing with water. For the biotin−streptavidin coupling reaction, similar procedures were applied by using fluorophore tagged streptavidin. Streptavidin conjugated Alexa Fluors 430 and 568 (Molecular Probes, green and red fluorophore, respectively) was reacted with biotin on viruses and then washed in water and dried with nitrogen. Notably, nonbuffered solutions of antibody and streptavidin were used to exclude any possibility of structural damage or charge rearrangements of an assembled film of polyelectrolyte multilayers and M13 viruses by high ionic strength of buffer solution. We used Tween 20 detergent (0.2 vol %) and a short time period (5 min) for binding to minimize any nonspecific (e.g., electrostatic or van der Waals interactions) binding of the antibody and streptavidin onto the polyelectrolyte multilayer and substrate. Control experiments were performed with bare films of polyelectrolyte multilayers (without viruses) and successfully confirmed that the fluorescence signal from nonspecific binding was relatively negligible.

Surface Characterization and Imaging. The patterned assembly of viruses was mainly characterized with AFM

(Digital Instruments, Dimension 3100 with Nanoscope IIIa controller). In order to minimize any possible misreading during data acquisition on topologically patterned surface and to enhance the image resolution, we used slow scanning tapping mode (0.5−1.0 Hz of scan speed) with supersharp silicon probes (Pacific Nanotechnology, SSS-NCH). A scanning electron microscope (JEOL) was used to obtain magnified cross-sectional images of patterned polyelectrolyte multilayers. Prior to imaging, 5 nm thicknesses of the Au layer were deposited on the surface to prevent charging.

Acknowledgment. This work was supported by the Army Research Office Institute of Soldier Nanotechnologies.

References

(1) Huang, Y.; Duan, X. F.; Wei, Q. Q.; Lieber, C. M. *Science* **2001**, *291*, 630–633.
(2) Patolsky, F.; Zheng, G. F.; Hayden, O.; Lakadamyali, M.; Zhuang, X. W.; Lieber, C. M. *Proc. Natl. Acad. Sci. U.S.A.* **2004**, *101*, 14017–14022.
(3) Kong, J.; Franklin, N. R.; Zhou, C. W.; Chapline, M. G.; Peng, S.; Cho, K. J.; Dai, H. J. *Science* **2000**, *287*, 622–625.
(4) Hartgerink, J. D.; Beniash, E.; Stupp, S. I. *Science* **2001**, *294*, 1684–1688.
(5) Park, S.; Lim, J. H.; Chung, S. W.; Mirkin, C. A. *Science* **2004**, *303*, 348–351.
(6) Wang, Y. H.; Maspoch, D.; Zou, S. L.; Schatz, G. C.; Smalley, R. E.; Mirkin, C. A. *Proc. Natl. Acad. Sci. U.S.A.* **2006**, *103*, 2026–2031.
(7) Meitl, M. A.; Zhou, Y. X.; Gaur, A.; Jeon, S.; Usrey, M. L.; Strano, M. S.; Rogers, J. A. *Nano Lett.* **2004**, *4*, 1643–1647.
(8) Mesquida, P.; Ammann, D. L.; MacPhee, C. E.; McKendry, R. A. *Adv. Mater.* **2005**, *17*, 893–897.
(9) Tsukruk, V. V.; Ko, H.; Peleshanko, S. *Phys. Rev. Lett.* **2004**, *92*, 065502.
(10) Ko, H.; Tsukruk, V. V. *Nano Lett.* **2006**, *6*, 1443–1448.
(11) Shim, B. S.; Kotov, N. A. *Langmuir* **2005**, *21*, 9381–9385.
(12) Flynn, C. E.; Lee, S. W.; Peelle, B. R.; Belcher, A. M. *Acta Mater.* **2003**, *51*, 5867–5880.
(13) Dogic, Z.; Fraden, S. *Curr. Opin. Colloid Interface Sci.* **2006**, *11*, 47–55.
(14) Lee, S. W.; Lee, S. K.; Belcher, A. M. *Adv. Mater.* **2003**, *15*, 689–692.
(15) Lee, S. W.; Mao, C. B.; Flynn, C. E.; Belcher, A. M. *Science* **2002**, *296*, 892–895.
(16) Cheung, C. L.; Camarero, J. A.; Woods, B. W.; Lin, T. W.; Johnson, J. E.; De Yoreo, J. J. *J. Am. Chem. Soc.* **2003**, *125*, 6848–6849.
(17) Lee, K. B.; Kim, E. Y.; Mirkin, C. A.; Wolinsky, S. M. *Nano Lett.* **2004**, *4*, 1869–1872.
(18) Yi, H. M.; Nisar, S.; Lee, S. Y.; Powers, M. A.; Bentley, W. E.; Payne, G. F.; Ghodssi, R.; Rubloff, G. W.; Harris, M. T.; Culver, J. N *Nano Lett.* **2005**, *5*, 1931–1936.
(19) Vega, R. A.; Maspoch, D.; Salaita, K.; Mirkin, C. A. *Angew. Chem., Int. Ed.* **2005**, *44*, 6013–6015.
(20) Cheung, C. L.; Chung, S. W.; Chatterji, A.; Lin, T. W.; Johnson, J. E.; Hok, S.; Perkins, J.; De Yoreo, J. J. *J. Am. Chem. Soc.* **2006**, *128*, 10801–10807.
(21) Decher, G. *Science* **1997**, *277*, 1232–1237.
(22) Hammond, P. T. *Adv. Mater.* **2004**, *16*, 1271–1293.
(23) Yoo, P. J.; Nam, K. T.; Qi, J. F.; Lee, S. K.; Park, J.; Belcher, A. M.; Hammond, P. T. *Nat. Mater.* **2006**, *5*, 234–240.
(24) Nam, K. T.; Kim, D. W.; Yoo, P. J.; Chiang, C. Y.; Meethong, N.; Hammond, P. T.; Chiang, Y. M.; Belcher, A. M. *Science* **2006**, *312*, 885–888.
(25) Jiang, X. P.; Zheng, H. P.; Gourdin, S.; Hammond, P. T. *Langmuir* **2002**, *18*, 2607–2615.
(26) Zheng, H. P.; Lee, I.; Rubner, M. F.; Hammond, P. T. *Adv. Mater.* **2002**, *14*, 569–572.
(27) Park, J.; Hammond, P. T. *Adv. Mater.* **2004**, *16*, 520–525.
(28) Kim, Y. S.; Baek, S. J.; Hammond, P. T. *Adv. Mater.* **2004**, *16*, 581–584.
(29) Park, J.; Fouche, L. D.; Hammond, P. T. *Adv. Mater.* **2005**, *17*, 2575–2579.
(30) Ko, H. H.; Jiang, C. Y.; Tsukruk, V. V. *Chem. Mater.* **2005**, *17*, 5489–5497.
(31) Hiller, J.; Mendelsohn, J. D.; Rubner, M. F. *Nat. Mater.* **2002**, *1*, 59–63.
(32) Jang, H.; Kim, S.; Char, K. *Langmuir* **2003**, *19*, 3094–3097.
(33) Zhang, L. L.; Peng, Z. H.; Yao, L. H.; Lv, F. Z.; Li, X. *J. Mater. Chem.* **2007**, *17*, 3015–3022.
(34) Hua, F.; Shi, J.; Lvov, Y.; Cui, T. *Nano Lett.* **2002**, *2*, 1219–1222.
(35) Mohammed, J. S.; DeCoster, M. A.; McShane, M. J. *Langmuir* **2006**, *22*, 2738–2746.
(36) Suh, K. Y.; Kim, Y. S.; Lee, H. H. *Adv. Mater.* **2001**, *13*, 1386–1389.
(37) Picart, C.; Mutterer, J.; Richert, L.; Luo, Y.; Prestwich, G. D.; Schaaf, P.; Voegel, J. C.; Lavalle, P. *Proc. Natl. Acad. Sci. U.S.A.* **2002**, *99*, 12531–12535.
(38) Lavalle, P.; Gergely, C.; Cuisinier, F. J. G.; Decher, G.; Schaaf, P.; Voegel, J. C.; Picart, C. *Macromolecules* **2002**, *35*, 4458–4465.
(39) Zacharia, N. S.; DeLongchamp, D. M.; Modestino, M.; Hammond, P. T. *Macromolecules* **2007**, *40*, 1598–1603.
(40) Shiratori, S. S.; Rubner, M. F. *Macromolecules* **2000**, *33*, 4213–4219.
(41) Suh, K. Y.; Lee, H. H. *Adv. Funct. Mater.* **2002**, *12*, 405–413.
(42) Suh, K. Y.; Kim, P.; Lee, H. H. *Appl. Phys. Lett.* **2004**, *85*, 4019–4021.
(43) Lutkenhaus, J. L.; Hrabak, K. D.; McEnnis, K.; Hammond, P. T. *J. Am. Chem. Soc.* **2005**, *127*, 17228–17234.
(44) Mallwitz, F.; Laschewsky, A. *Adv. Mater.* **2005**, *17*, 1296–1299.
(45) Kim, Y. S.; Suh, K. Y.; Lee, H. H. *Appl. Phys. Lett.* **2001**, *79*, 2285–2287.
(46) Khang, D. Y.; Lee, H. H. *Appl. Phys. Lett.* **2000**, *76*, 870–872.
(47) Reiter, G. *Phys. Rev. Lett.* **1992**, *68*, 75–78.
(48) Lenz, P. *Adv. Mater.* **1999**, *11*, 1531–1534.
(49) Bicerano, J. *Prediction of Polymer Properties*, 2nd ed.; Marcel Dekker, Inc.: New York, 1996; pp 162–173..
(50) Velikov, V.; Borick, S.; Angell, C. A. *Science* **2001**, *294*, 2335–2338.
(51) Sharp, J. S.; Jones, R. A. L. *Phys. Rev. E* **2002**, *66*, 011801.

NL073079F